
Ergodic variational flows

Zuheng Xu Naitong Chen Trevor Campbell

Department of Statistics

University of British Columbia

[zuheng.xu | naitong.chen | trevor]@stat.ubc.ca

Abstract

This work presents a new class of variational family—*ergodic variational flows*—that not only enables tractable i.i.d. sampling and density evaluation, but also comes with MCMC-like convergence guarantees. Ergodic variational flows consist of a mixture of repeated applications of a measure-preserving and ergodic map to an initial reference distribution. We provide mild conditions under which the variational distribution converges weakly and in total variation to the target as the number of steps in the flow increases; this convergence holds regardless of the value of variational parameters, although different parameter values may result in faster or slower convergence. Further, we develop a particular instantiation of the general family using Hamiltonian dynamics combined with deterministic momentum refreshment. Simulated and real data experiments provide an empirical verification of the convergence theory and demonstrate that samples produced by the method are of comparable quality to a state-of-the-art MCMC method.

1 Introduction

Bayesian statistical modelling and inference provides a principled approach to learning from data. However, for all but the simplest models, exact inference is not possible and computational approximations are required. A standard methodology for Bayesian inference is Markov chain Monte Carlo (MCMC) [1; 2; 3, Ch. 11,12], which involves simulating a Markov chain whose stationary distribution is the Bayesian posterior distribution, and then treating the sequence of states as draws from the posterior. MCMC methods are supported by theory that guarantees that if one simulates the chain for long enough, Monte Carlo averages based on the sequence of states will converge to the exact posterior expectation of interest (see, e.g., [4]). This “exactness” property is quite compelling: regardless of how well one is able to tune the Markov chain, the method is guaranteed to eventually produce an accurate result given enough computation time. Nevertheless, it remains a challenge to assess the performance of MCMC in practice with a finite computational budget. One option is to use a Stein discrepancy [5–9], which provides a metric that quantifies how well a set of MCMC samples approximates the posterior distribution. But Stein discrepancies are unreliable in the presence of multimodality [10], suffer from the curse of dimensionality [11], and are often computationally expensive to estimate [12]. The other option is to use a traditional diagnostic, e.g., Gelman–Rubin [13, 14], effective sample size [3, p. 286], Geweke [15], and others [16]. These diagnostics are helpful in detecting mixing issues, but do not comprehensively quantify how well the MCMC samples approximate the posterior.

Variational inference (VI) [17–19] is an alternative to MCMC that does provide a straightforward quantification of posterior approximation error. In particular, VI involves approximating the posterior with a probability distribution—typically selected from a parametric family—that enables both i.i.d. sampling and density evaluation [18, 20–22]. Because one can take i.i.d. draws and evaluate the density, one can estimate the Kullback-Leibler (KL) divergence [23] to the posterior up to a constant (i.e., the ELBO [19]). The ability to estimate the ELBO, in turn, enables scalable tuning

via straightforward stochastic gradient descent algorithms [24, 25], optimally mixed approximations [26–34], model selection [35–40], and more. However, VI typically does not possess the same “exactness regardless of tuning” that MCMC does. The optimal variational distribution is not usually equal to the posterior due to the use of a limited parametric variational family; and even if it were, one could not reliably find it in general due to nonconvexity of the KL objective [41]. A recent line of work has begun to address this problem by constructing variational families from parametrized Markov chains targeting the posterior. Many are related to annealed importance sampling [42–47]; these methods introduce numerous auxiliary random variables and only have convergence guarantees in the limit of increasing dimension of the joint distribution. Those based on normalizing flows [48–50] avoid the increase in dimension with flow length, but typically do not have guaranteed convergence to the target. Methods involving the final-state marginal of finite simulations of standard MCMC methods do not enable tractable density evaluation [51].

In this work, we introduce a variational flow family—*ergodic variational flows*—that provide both MCMC-like convergence guarantees and tractable i.i.d. sampling and density evaluation (and hence ELBO estimation). Ergodic variational flows are constructed by mixing over repeated application of a measure-preserving, ergodic map. Our main theoretical results (Theorems 3.1 and 3.2) provide mild conditions under which the variational distribution converges weakly and in total variation to the target as the number of flow steps increases. Since these results hold for any value of the variational parameter, we are assured that our method targets the right distribution regardless of the result of tuning—as in MCMC. But since we can take i.i.d. draws and evaluate the density, we have access to the ELBO, which enables parameter optimization, comparison of multiple flows, optimal mixtures of multiple flows, and more. We present a specific instantiation of the general methodology based on Hamiltonian dynamics, with a discretization that can be tuned by maximizing the ELBO. Simulated and real data experiments verify the convergence of ergodic variational flows and demonstrate a comparable output sample quality to the No-U-Turn sampler [52].

2 Background

2.1 Variational inference with flows

Consider a set $\mathcal{X} \subseteq \mathbb{R}^d$ endowed with its Borel σ -algebra, and a target probability distribution π on \mathcal{X} whose density with respect to the Lebesgue measure we denote $\pi(x)$ for $x \in \mathcal{X}$. In the setting of Bayesian inference, π is the posterior distribution that we aim to approximate, and we are only able to evaluate a function $p(x)$ such that $p(x) = Z \cdot \pi(x)$ for some unknown normalization constant $Z > 0$. Throughout, we will assume all distributions have densities with respect to the Lebesgue measure on \mathcal{X} , and will use the same symbol to denote a distribution and its density; it will always be clear from context what is meant. The ideas in this work extend naturally to a more general setting, but we focus on this setup for simplicity.

Variational inference involves approximating the target distribution π by minimizing the Kullback-Leibler (KL) divergence from π to members of a parametric family $\{q_\lambda : \lambda \in \Lambda\}$, $\Lambda \subseteq \mathbb{R}^p$, i.e.,

$$\lambda^* = \arg \min_{\lambda \in \Lambda} D_{\text{KL}}(q_\lambda || \pi) = \arg \min_{\lambda \in \Lambda} \int q_\lambda(x) \log \frac{q_\lambda(x)}{p(x)} dx. \quad (1)$$

The two objective functions in Eq. (1) differ only by the constant $\log Z$. In order to be able to optimize λ using standard techniques, the variational family of distributions q_λ , $\lambda \in \Lambda$ must enable both i.i.d. sampling and density evaluation. A common approach to constructing such a family is to pass draws from a simple reference distribution q_0 through a measurable function $T_\lambda : \mathcal{X} \rightarrow \mathcal{X}$; T_λ is often referred to as a *flow* when comprised of repeated composed functions [20, 53, 54]. If T_λ is differentiable, invertible, and has a differentiable inverse, then we can express the density of the transformed variable $X = T_\lambda(Y)$, $Y \sim q_0$ as

$$\forall x \in \mathcal{X} \quad q_\lambda(x) = \frac{q_0(T_\lambda^{-1}(x))}{J_\lambda(T_\lambda^{-1}(x))} \quad J_\lambda(x) = |\det \nabla_x T_\lambda(x)|. \quad (2)$$

In this case the optimization in Eq. (1) can be rewritten using a transformation of variables as

$$\lambda^* = \arg \min_{\lambda \in \Lambda} \int q_0(x) \log \frac{q_0(x)}{J_\lambda(x)p(T_\lambda(x))} dx. \quad (3)$$

One can solve the optimization problem Eq. (3) using unbiased stochastic estimates of the gradient¹ with respect to λ based on draws from q_0 [55, 56],

$$\nabla_{\lambda} D_{\text{KL}}(q_{\lambda} || \pi) \approx \nabla_{\lambda} \log \frac{q_0(X)}{J_{\lambda}(X)p(T_{\lambda}(X))}, \quad X \sim q_0. \quad (4)$$

One can optionally reduce the variance of the above estimate by averaging over multiple samples $(X_j)_{j=1}^J \stackrel{\text{i.i.d.}}{\sim} q_0$ or by including a control variate [25]. The map T_{λ} is often complicated, and so automatic differentiation [57] is used to compute the derivatives in Eq. (4).

2.2 Measure-preserving and ergodic maps

Variational flows are often constructed from a flexible, general-purpose parametrized family $\{T_{\lambda} : \lambda \in \Lambda\}$ that is not specialized for any particular target distribution [22]; it is the job of the KL divergence minimization Eq. (3) to adapt the parameter λ such that q_{λ} becomes a good approximation of the target π . However, there are certain functions—in particular, those that are both *measure-preserving* and *ergodic* for π —that naturally provide a means to approximate expectations of interest under π without the need for tuning. Intuitively, a measure-preserving map T will not change the distribution of draws from π : if $X \sim \pi$, then $T(X) \sim \pi$. And an ergodic map T , when applied repeatedly, will not get “stuck” in a subset of \mathcal{X} unless it has probability either 0 or 1 under π . The precise definitions are given in Definitions 2.1 and 2.2.

Definition 2.1 (Measure-preserving map [58, pp. 73, 105]). *A measurable function $T : \mathcal{X} \rightarrow \mathcal{X}$ is measure-preserving for π if $T\pi = \pi$, where $T\pi$ is the pushforward measure given by $\pi(T^{-1}(A))$ for each measurable set $A \subseteq \mathcal{X}$.*

Definition 2.2 (Ergodic map [58, pp. 73, 105]). *A measurable function $T : \mathcal{X} \rightarrow \mathcal{X}$ is ergodic for π if for all measurable sets $A \subseteq \mathcal{X}$, $T(A) = A$ implies that $\pi(A) \in \{0, 1\}$.*

If a map T satisfies both Definitions 2.1 and 2.2, then long-run averages resulting from repeated applications of T will eventually converge to expectations under π , as shown by Theorem 2.3. When \mathcal{X} is compact, this result can be interpreted as showing that the discrete measure $\frac{1}{N} \sum_{n=0}^{N-1} \delta_{T^n x}$ converges weakly to π [59, Theorem 6.1.7].

Theorem 2.3 (Pointwise Ergodic Theorem [60; 58, p. 212]). *Suppose $T : \mathcal{X} \rightarrow \mathcal{X}$ is measure-preserving and ergodic for π , and $f \in L^1(\pi)$. Then*

$$\lim_{N \rightarrow \infty} \frac{1}{N} \sum_{n=0}^{N-1} f(T^n x) = \int f d\pi \quad \pi\text{-a.e. } x \in \mathcal{X}.$$

Fig. 1a provides an example illustration of this result when π is the uniform distribution $\text{Unif}[0, 1]$, $T : [0, 1] \rightarrow [0, 1]$ is the shift map $T(x) = x + \lambda \pmod{1}$ for some $\lambda \in \mathbb{R}$, and x is initialized at 0.5. In particular, for any irrational $\lambda \in \mathbb{R}$ (here $\pi/16$), the shift map is both measure-preserving and ergodic for π . As the number of applications increases, the collection of iterates $(T^n x)_{n=1}^N$ forms a discrete approximation to $\text{Unif}[0, 1]$. On the other hand, for a rational $\lambda \in \mathbb{R}$ (here $1/4$), the shift map is measure-preserving but not ergodic. In this case the iterates are trapped in the finite set $\{0, 0.25, 0.5, 0.75, 1\}$ and do not well-approximate $\text{Unif}[0, 1]$.

3 Ergodic variational flows

In this section, we develop a parametrized family of *ergodic variational flows* that enable tractable i.i.d. sampling, tractable density evaluation, and are guaranteed to converge to the target distribution both weakly and in total variation in the limit of increasingly many flow steps (Theorems 3.1 and 3.2) regardless of parameter tuning effort. Thus, ergodic variational flows provide the same compelling convergence result as MCMC, but with the added benefit of i.i.d. sampling and density evaluation, and hence unbiased estimates of the ELBO.

¹We assume throughout that differentiation and integration can be swapped wherever necessary.

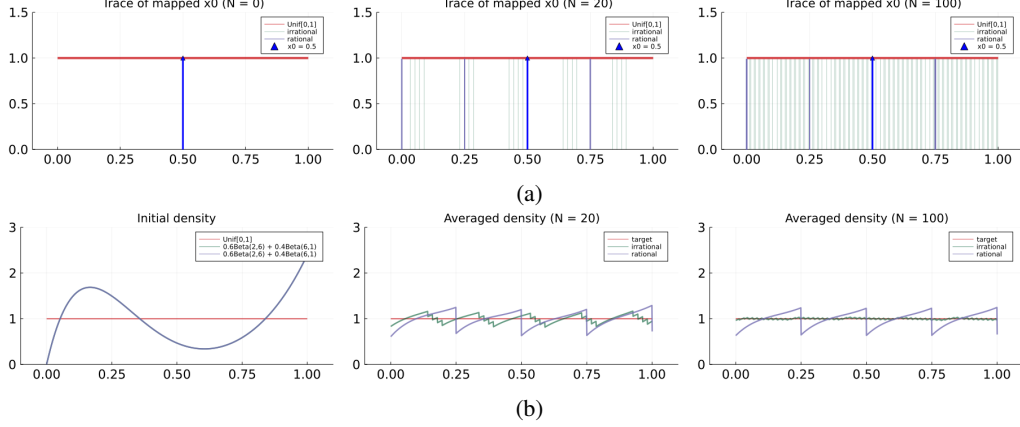


Figure 1: An illustration of the effect of the shift map $T(x) = x + \lambda \bmod 1$ for shift $\lambda \in \mathbb{R}$. Note that T is measure-preserving for $\pi = \text{Unif}[0, 1]$. Green denotes a case where λ is irrational ($\lambda = \pi/16$), blue denotes a case where λ is rational ($\lambda = 1/4$), and the red horizontal line shows the uniform density. (1a): Starting from $x = 0.5$, repeated application of an irrational shift map eventually creates a discrete probability measure that converges weakly to $\text{Unif}[0, 1]$; the rational shift map is periodic and so does not exhibit this behaviour. (1b): Starting from a mixture of beta distributions, averaging over repeated applications of the shift map does converge to $\text{Unif}[0, 1]$ in total variation when λ is irrational.

3.1 Variational family

Define a reference distribution q_0 on \mathcal{X} for which i.i.d. sampling and density evaluation is tractable, and a collection of measurable functions $T_\lambda : \mathcal{X} \rightarrow \mathcal{X}$ parametrized by $\lambda \in \Lambda$ such that for each parameter value λ , the map T_λ is measure-preserving and ergodic for π . Then the *ergodic variational flow family* generated by q_0 and T_λ is the collection of distributions

$$q_{\lambda, N} = \frac{1}{N} \sum_{n=0}^{N-1} T_\lambda^n q_0 \quad \text{for} \quad \lambda \in \Lambda, N \in \mathbb{N},$$

where $T_\lambda^n q_0$ denotes the pushforward of the distribution q_0 under n repeated applications of T_λ . Although novel in the context of Bayesian variational inference, this type of mixed ergodic average distribution has been previously studied in the probability theory literature [61, 62]. Similar mixed averages of pushforward distributions have also appeared in recent work on importance sampling using the orbit of deterministic transforms [63, 64].

Fig. 1b displays a simple example of this family where q_0 is a mixture of beta distributions $q_0 = 0.6 \cdot \text{Beta}(2, 6) + 0.4 \cdot \text{Beta}(6, 1)$ and T_λ is the shift map $T_\lambda(x) = x + \lambda \bmod 1$ for shift $\lambda = \pi/16$. Because T_λ is measure-preserving and ergodic for $\text{Unif}[0, 1]$, the uniformly-weighted average of $T_\lambda^n q_0$ from $n = 0, \dots, N$ converges in total variation to $\text{Unif}[0, 1]$, despite starting at some other arbitrary distribution q_0 . In fact, any irrational λ will provide the same result (although the speed of convergence of $q_{\lambda, N}$ to $\text{Unif}[0, 1]$ will depend on λ). Thus, in this example, the proposed ergodic variational flow family $\{q_{\lambda, N} : \lambda \in \Lambda, N \in \mathbb{N}\}$ achieves the same ‘‘convergence regardless of tuning’’ enjoyed by MCMC methods. The theory in Section 3.2 shows that this result extends generally.

3.2 Convergence guarantees

In this section, we show that for all $\lambda \in \Lambda$, the distribution $q_{\lambda, N}$ converges to π as $N \rightarrow \infty$ (proofs may be found in Appendix A). Thus, regardless of the ability to tune the parameter λ , we are guaranteed that $q_{\lambda, N}$ can arbitrarily approximate π given enough computational effort (i.e., large enough N). In particular, we demonstrate this convergence in three senses: weak, setwise, and in total variation. Recall that a sequence of probability distributions q_n converges *weakly* to π if

$$\forall \text{ bounded, continuous } f : \mathcal{X} \rightarrow \mathbb{R}, \quad \lim_{n \rightarrow \infty} \int f(x) q_n(dx) = \int f(x) \pi(dx),$$

Algorithm 1 `Sample`($q_{\lambda,N}$): Take a draw from $q_{\lambda,N}$.

Require: reference distribution q_0 , flow map T_λ , number of steps N
 $K \leftarrow \text{Sample}(\text{Unif}\{0, 1, \dots, N\})$
 $x_0 \leftarrow \text{Sample}(q_0)$
return $T_\lambda^K(x_0)$

Algorithm 2 `log` $q_{\lambda,N}(x)$: Evaluate the log-density of $q_{\lambda,N}$ at $x \in \mathcal{X}$.

Require: location x , reference distribution q_0 , flow map T_λ , Jacobian J_λ , number of steps N
 $\log J = 0$
 $\log f_0 \leftarrow \log q_0(x)$
for $n = 1, \dots, N - 1$ **do**
 $x \leftarrow T_\lambda^{-1}(x)$
 $\log J \leftarrow \log J + \log J_\lambda(x)$
 $\log f_n \leftarrow \log q_0(x) - \log J$
end for
return $\text{LogSumExp}(\log f_0, \dots, \log f_{N-1}) - \log N$

Algorithm 3 `EstELBO`(λ, N): Obtain an unbiased estimate of the ELBO for $q_{\lambda,N}$.

Require: reference q_0 , unnormalized target p , flow map T_λ , Jacobian J_λ , number of flow steps N
 $x \leftarrow \text{Sample}(q_{\lambda,N})$
return $\log p(x) - \log q_{\lambda,N}(x)$

and converges *setwise* to π if

$$\forall \text{measurable } A \subseteq \mathcal{X}, \quad \lim_{n \rightarrow \infty} q_n(A) = \pi(A).$$

Theorem 3.1. *Suppose $q_0 \ll \pi$ and T_λ is measure-preserving and ergodic for π . Then $q_{\lambda,N}$ converges both setwise and weakly to π as $N \rightarrow \infty$.*

We obtain a stronger result—convergence in total variation—when we can express the density of $q_{\lambda,N}$ using the usual transformation of variables formula Eq. (2). Recall that a sequence of distributions q_n converges in *total variation* to π if $D_{\text{TV}}(q_n, \pi) \rightarrow 0$ as $n \rightarrow \infty$, where

$$D_{\text{TV}}(q, \pi) = \sup_A |q(A) - \pi(A)| = \sup_{f: \mathcal{X} \rightarrow [0,1]} |\mathbb{E}[f(X)] - \mathbb{E}[f(Y)]| = \frac{1}{2} \int |q(x) - \pi(x)| dx.$$

Theorem 3.2. *Suppose $q_0 \ll \pi$, T_λ is a diffeomorphism, and T_λ is measure-preserving and ergodic for π . Then $q_{\lambda,N}$ converges in total variation to π as $N \rightarrow \infty$.*

This result is asymptotic in nature, which suffices for our purposes to guarantee that the family can well-approximate the target π in the large- N limit; in practice we use the ELBO (see Section 3.4) to tune λ and N . However, similar nonasymptotic results exist under stronger technical conditions (finite state space or minorization and drift conditions) [61]. It is also worth noting that while Theorem 3.2 pertains to the total variation distance, the KL divergence is more relevant in the context of variational inference. However, a small total variation distance implies a small KL divergence in many practical scenarios, e.g., when the density ratio $q(x)/\pi(x)$ is bounded (Proposition A.2 [65, Theorem 7]).

3.3 Sampling and density evaluation

We can obtain an independent draw $X \sim q_{\lambda,N}$ by treating $q_{\lambda,N}$ as a mixture of N distributions:

$$K \sim \text{Unif}\{0, 1, \dots, N - 1\} \quad X_0 \sim q_0 \quad X = T_\lambda^K(X_0).$$

The procedure is given in Algorithm 1. On average, this computation requires $\mathbb{E}[K] = \frac{N-1}{2}$ applications of T_λ , and at most it requires $N - 1$ applications. If $T_\lambda : \mathcal{X} \rightarrow \mathcal{X}$ is differentiable with

Jacobian $J_\lambda : \mathcal{X} \rightarrow \mathbb{R}$ and has a differentiable inverse, we can also express the density of $q_{\lambda,N}$ by using a transformation of variables formula on each component in the mixture:

$$q_{\lambda,N}(x) = \frac{1}{N} \sum_{n=0}^{N-1} \frac{q_0(T_\lambda^{-n}x)}{\prod_{j=1}^n J_\lambda(T_\lambda^{-j}x)}.$$

This density can be computed efficiently using $N - 1$ evaluations of T_λ^{-1} and J_λ each; the procedure to compute $\log q_{\lambda,N}$ is given in Algorithm 2.

3.4 ELBO estimation

We can minimize the KL divergence from $q_{\lambda,N}$ to π by maximizing the ELBO [19], given by

$$\begin{aligned} \text{ELBO}(\lambda, N) &= \int q_{\lambda,N}(x) \log \frac{p(x)}{q_{\lambda,N}(x)} dx \\ &= \int \frac{1}{N} \sum_{n=0}^{N-1} \frac{q_0(T_\lambda^{-n}x)}{\prod_{j=1}^n J_\lambda(T_\lambda^{-j}x)} \log \frac{p(x)}{q_{\lambda,N}(x)} dx \\ &= \frac{1}{N} \sum_{n=0}^{N-1} \int q_0(x) \log \frac{p(T_\lambda^n x)}{q_{\lambda,N}(T_\lambda^n x)} dx. \end{aligned}$$

Therefore we can obtain an unbiased estimate of the ELBO using the following procedure:

$$K \sim \text{Unif}\{0, \dots, N-1\} \quad X_0 \sim q_0 \quad X = T_\lambda^K(X_0) \quad \widehat{\text{ELBO}}(\lambda, N) = \log p(X) - \log q_{\lambda,N}(X),$$

which has the same cost as taking a single draw from $q_{\lambda,N}$ and evaluating its density. The procedure is given in Algorithm 3. Note that the pseudocode in Algorithm 3 wastes some computation, since the original forward map by K applications of T_λ will be reversed by $N - 1$ steps when evaluating the log density $\log q_{\lambda,N}(X)$ via Algorithm 2. In practice, one can avoid this wasted computation by precomputing $T_\lambda^{K-(N-1)}x, T_\lambda^{K-(N-2)}x, \dots, x, T_\lambda x, T_\lambda^2 x, \dots, T_\lambda^K x$ and passing all of these into the function that computes $\log q_{\lambda,N}$ (instead of looping $x \leftarrow T_\lambda^{-1}x$ repeatedly).

3.5 Numerical stability

Density evaluation (Algorithm 2) and ELBO estimation (Algorithm 3) both involve repeated applications of T_λ and T_λ^{-1} . This poses no issue in theory, but in a computer—where floating point computations are used—it is critical to code the map T_λ and its inverse T_λ^{-1} in a numerically precise way such that the composition of $(T_\lambda^K) \circ (T_\lambda^{-K})$ is the identity map for large $K \in \mathbb{N}$. In practice, we check the limits of stability of our flow implementation by taking draws from q_0 and evaluating T_λ^K followed by T_λ^{-K} (and vice versa) for increasing K until we cannot reliably invert the flow. See Fig. 6 in the appendix for an example usage of this diagnostic. Note that for sample generation specifically (Algorithm 1), however, numerical stability is not as much of a concern as it only requires repeated forward evaluation of the map T_λ .

4 Hamiltonian ergodic variational flows

In this section, we provide a particular instance of an ergodic variational flow based on Hamiltonian dynamics. In particular, consider the *augmented* target density on $\mathcal{X} \times \mathbb{R}^d \times [0, 1]$,

$$\bar{\pi}(x, \rho, u) = \pi(x) \cdot m(\rho) \cdot \mathbf{1}[0 \leq u \leq 1], \quad m(\rho) = \prod_{i=1}^d r(\rho_i),$$

with auxiliary variables $\rho \in \mathbb{R}^d$, $u \in [0, 1]$, and some almost-everywhere differentiable univariate probability density $r : \mathbb{R} \rightarrow \mathbb{R}_+$. The x -marginal distribution of $\bar{\pi}$ is the original target distribution π ; therefore if we are able to obtain i.i.d. draws from $\bar{\pi}$, we can obtain i.i.d. draws from π by simply discarding the ρ and u components. We construct a measure-preserving and ergodic map T by composing the following three steps in sequence:

(1) Hamiltonian dynamics We first apply

$$(x', \rho') \leftarrow H_t(x, \rho),$$

where $H_t : \mathcal{X} \times \mathbb{R}^d \rightarrow \mathcal{X} \times \mathbb{R}^d$ is the map of Hamiltonian dynamics with position x and momentum ρ simulated for an interval of length $t \in \mathbb{R}_+$,

$$\frac{d\rho}{dt} = \nabla \log \pi(x) \qquad \frac{dx}{dt} = -\nabla \log m(\rho). \quad (5)$$

One can show that this preserves density (and hence is measure preserving) and it is also unit Jacobian [66]. In practice, one approximately simulates the dynamics in Eq. (5) by running L steps of the leapfrog method, which involves interleaving three discrete transformations with step size $\epsilon > 0$,

$$\begin{aligned} \hat{\rho}_{k+1} &= \rho_k + \frac{\epsilon}{2} \nabla \log \pi(x_k) \\ x_{k+1} &= x_k - \epsilon \nabla \log m(\hat{\rho}_{k+1}) \\ \rho_{k+1} &= \hat{\rho}_{k+1} + \frac{\epsilon}{2} \nabla \log \pi(x_{k+1}) \end{aligned} \quad (6)$$

Denote the map constructed by applying these three steps in sequence $\hat{H}_\epsilon : \mathbb{R}^{2d} \rightarrow \mathbb{R}^{2d}$. As the transformations in Eq. (6) are all shear, \hat{H}_ϵ is also unit Jacobian, and for small enough step size ϵ it nearly maintains the target invariance. Although this map is no longer exactly measure-preserving, it is in the limit as $\epsilon \rightarrow 0$, and we can tune the step size ϵ in practice via ELBO maximization.

(2) Pseudotime shift Second, we apply a constant shift to the pseudotime variable u ,

$$u' \leftarrow u + \xi \pmod{1},$$

where $\xi \in \mathbb{R}$ is a fixed irrational number (say, $\xi = \pi/16$). As this is a constant shift, it is unit Jacobian and density-preserving (and hence measure-preserving). The u component will behave like a notion of “time” of the flow, and essentially ensures that the refreshment of ρ in step (3) below will take a different form even if x visits the same location again.

(3) Momentum refreshment Finally, we refresh the momentum variables via

$$\forall i = 1, \dots, d, \quad \rho_i'' \leftarrow R^{-1}(R(\rho_i') + z(x_i', u')) \pmod{1},$$

where R is the cumulative distribution function (CDF) of density r , and $z : \mathcal{X} \times [0, 1] \rightarrow \mathbb{R}$ is a differentiable “pseudorandom” function, e.g., $z(x_i, u) = \sin(ax_i + u)$ for some large value of $a \in \mathbb{R}$; this generalizes the map from [67, 68] to enable the shift to depend on the state x and pseudotime u . This map is measure-preserving as it involves mapping the momentum to a $\text{Unif}[0, 1]$ random variable via the CDF, shifting by an amount that only depends on x, u , and then mapping back using the inverse CDF. The Jacobian is the joint momentum density ratio $m(\rho')/m(\rho'')$.

The composition of these three steps to compute T_λ and its Jacobian J_λ is given in Algorithm 4 in Appendix B. One can view T_λ as being similar to a single iteration of uncorrected Hamiltonian Monte Carlo (HMC) [66, 69]. Step (1) is identical to the Hamiltonian dynamics simulation in HMC, while steps (2-3) essentially attempt to replicate the independent resampling of $\rho \sim m$ using only deterministic maps. Note that the parameter λ of this overall map consists of the step size ϵ and number of leapfrog steps L , which both can be optimized.

5 Experiments

In this section, we demonstrate the approximation capabilities of Hamiltonian ergodic variational flows (ErgFlow) on synthetic and real data examples. We also compare the sample quality of ErgFlow against 5,000 samples from the No-U-Turn sampler (NUTS) [52]. Since NUTS does not enable density evaluation, we compare using a kernel Stein discrepancy (KSD) [6, 7]. For all experiments, we use the standard Laplace distribution as the momentum distribution; although Gaussians are more commonly used in HMC, we find that the Laplace was more numerically stable to work with (see Fig. 6 in Appendix D). More experimental details may be found in Appendix D. All experiments were conducted on a machine with an AMD Ryzen 9 3900X and 32GB of RAM.

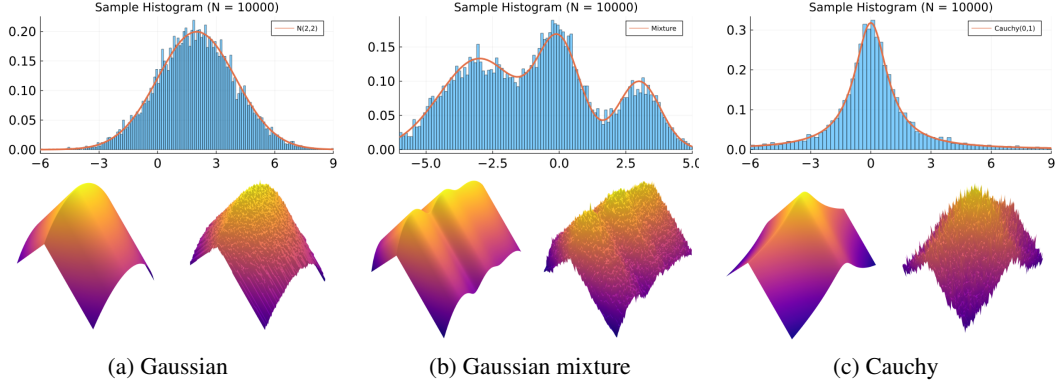


Figure 2: Marginal sample histograms (first row) and pairs of exact and approximate joint log density (second row) for Gaussian (2a), mixture (2b), and Cauchy (2c) targets.

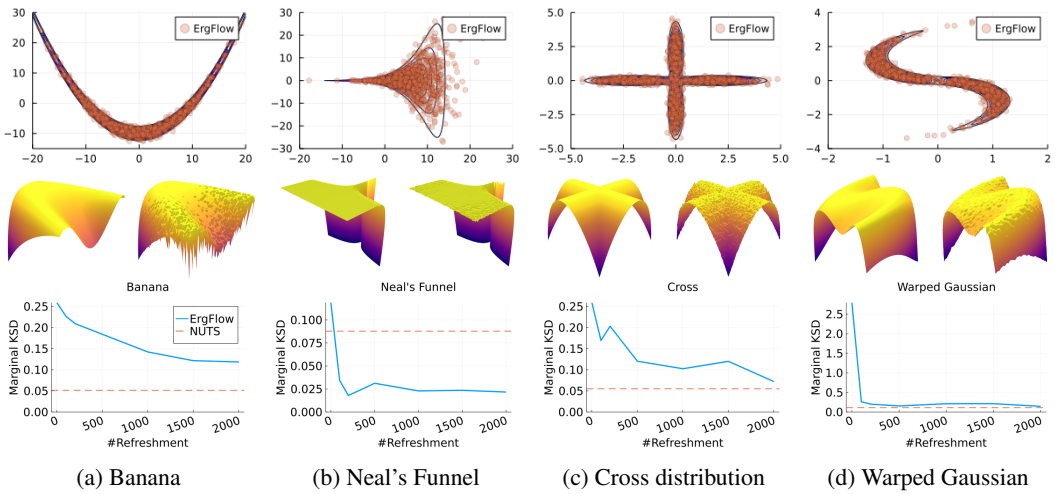


Figure 3: Marginal sample histograms (first row), pairs of sliced exact and approximate joint log density (second row), and KSD comparison with 5,000 samples from the No-U-Turn sampler [24] for banana (3a), funnel (3b), cross (3c), and warped Gaussian (3d) targets.

5.1 Univariate synthetic example

We begin by providing a qualitative examination of the i.i.d. samples and the approximated targets produced by ErgFlow initialized at $q_0 = \mathcal{N}(0, 1)$ for three one-dimensional synthetic distributions: a Gaussian, a mixture of Gaussians, and the standard Cauchy. We excluded the pseudotime variable u in these tests, such that we could visualize the full joint density of (x, ρ) in 2 dimensions. More details can be found in Appendix D.1. Figs. 2a to 2c show histograms of 10,000 i.i.d. x -marginal samples generated by ErgFlow for each of the three targets, all of which nearly perfectly match the true target marginal densities. Figs. 2a to 2c also shows that the ErgFlow joint density $\log q_{\lambda, N}$ is generally a good approximation of the log joint target density. These results confirm our theory in Section 3.2 that ErgFlow exhibits MCMC-type convergence without sacrificing density evaluation.

5.2 Multidimensional synthetic example

Next, we test ErgFlow on four challenging synthetic target distributions: the banana [70], Neal's funnel [71], a cross-shaped Gaussian mixture, and a warped Gaussian. All four examples have a 2-dimensional state $x \in \mathbb{R}^2$, and hence $(x, \rho, u) \in \mathbb{R}^5$. In each test we set the initial distribution q_0 to be the mean-field Gaussian approximation. More details can be found in Appendix D.2. Fig. 3 shows the scatter plots consisting of 1,000 i.i.d. x -marginal samples drawn from ErgFlow, as well as the approximated ErgFlow log density and exact log density, for each of the four targets. Note that

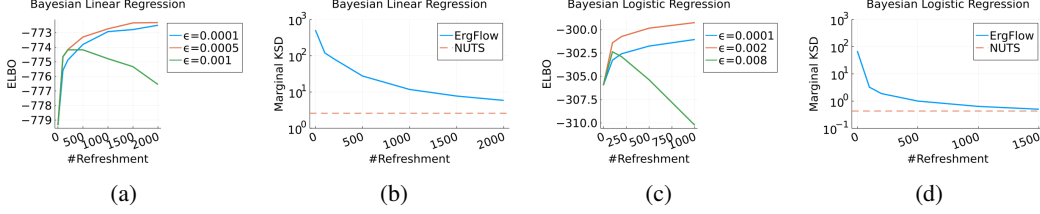


Figure 4: ELBO versus step size ϵ (Figs. 4a and 4c) and KSD comparison with NUTS (Figs. 4b and 4d) for the linear and logistic regression experiments.

because $(x, \rho, u) \in \mathbb{R}^5$, in order to visualize the log density Fig. 3 shows sliced log densities as a function of $x \in \mathbb{R}^2$ for a single value of (ρ, u) chosen randomly via $(\rho, u) \sim \text{Lap}(0, I) \times \text{Unif}[0, 1]$. We see that, qualitatively, both the samples and approximated densities produced by ErgFlow closely match those of the targets. The KSD comparison with NUTS provides a quantitative confirmation.

Additional results are provided in Appendix D.2. In particular, Figs. 5a and 5b show that one can tune the step size ϵ in the flow by maximizing the ELBO. We observe that overly large step sizes typically result in errors incurred by the use of discretized Hamiltonian dynamics, while small step sizes result in a flow that makes slow progress towards the target; both effects are evident from the ELBO. Furthermore, Fig. 6 uses the diagnostic from Section 3.5 to provide a comparison of the numerical stability of the flow when using a Laplace versus Gaussian momentum distribution. Finally, Fig. 7 provides a more comprehensive set of sample histograms for these experiments (showing the x -, ρ -, and u -marginals), and Fig. 8 shows that similar results as in Fig. 3 hold for higher-dimensional funnel examples (specifically 5- and 20-dimensional).

5.3 Bayesian linear and logistic regression

Finally, we test ErgFlow on Bayesian linear and logistic regression using two sets of real data. The two statistical models take the following form:

$$\textbf{Linear Reg.}: \beta, \log \sigma^2 \stackrel{\text{i.i.d.}}{\sim} \mathcal{N}(0, 1), \quad y_j | \beta, \sigma^2 \stackrel{\text{indep}}{\sim} \mathcal{N}(x_j^T \beta, \sigma^2)$$

$$\textbf{Logistic Reg.}: \alpha \sim \text{Gam}(1, 0.01), \quad \beta | \alpha \sim \mathcal{N}(0, \alpha^{-1} I), \quad y_j | \beta \stackrel{\text{indep}}{\sim} \text{Bern}\left(\frac{1}{1 + e^{-x_j^T \beta}}\right),$$

where y_j is the response and $x_j \in \mathbb{R}^p$ is the feature vector for data point j . For linear regression, we use the Boston housing prices dataset [72],² containing $J = 506$ suburbs/towns in the Boston area; the goal is to use suburb information to predict the median house price. For logistic regression, we use a bank marketing dataset [73] downsampled to $J = 400$ data points;³ the goal is to use client information to predict whether they subscribe to a term deposit. The overall (x, ρ, u) state dimension of the linear and logistic regression inference problems are 31 and 19, respectively. More experimental details may be found in Appendix D.3. Figs. 4a and 4c show the estimated ELBO across refreshments for various step sizes, and Figs. 4b and 4d compare the marginal KSD values across refreshments against that of NUTS. We observe the same effect that the step sizes have on the estimated ELBO values as in Section 5.2. And with an appropriate choice of step size, the sample qualities are comparable to those obtained using NUTS.

6 Conclusion

This work presented ergodic variational flows, a new variational family for distribution approximation that not only enables tractable i.i.d. sampling and density evaluation, but also comes with MCMC-like convergence guarantees. In particular, we provide conditions under which a flow constructed using a measure-preserving and ergodic map will converge weakly, setwise, and in total variation to the target distribution. Future work includes developing more stable momentum refreshment schemes, combining this work with coreset flow approaches to address computational cost in the large-data regime [47, 50], and examining extensions using ideas from involutive MCMC [74–76].

²Available in the MLDataSets Julia package at <https://github.com/JuliaML/MLDataSets.jl>.

³Available at <https://archive.ics.uci.edu/ml/datasets/bank+marketing>.

Acknowledgments and Disclosure of Funding

All authors were supported by a National Sciences and Engineering Council of Canada (NSERC) Discovery Grant and a gift from Google LLC.

References

- [1] Christian Robert and George Casella. *Monte Carlo Statistical Methods*. Springer, 2nd edition, 2004.
- [2] Christian Robert and George Casella. A short history of Markov Chain Monte Carlo: subjective recollections from incomplete data. *Statistical Science*, 26(1):102–115, 2011.
- [3] Andrew Gelman, John Carlin, Hal Stern, David Dunson, Aki Vehtari, and Donald Rubin. *Bayesian data analysis*. CRC Press, 3rd edition, 2013.
- [4] Gareth Roberts and Jeffrey Rosenthal. General state space Markov chains and MCMC algorithms. *Probability Surveys*, 1:20–71, 2004.
- [5] Jackson Gorham and Lester Mackey. Measuring sample quality with Stein’s method. In *Advances in Neural Information Processing Systems*, 2015.
- [6] Qiang Liu, Jason Lee, and Michael Jordan. A kernelized Stein discrepancy for goodness-of-fit tests and model evaluation. In *International Conference on Machine Learning*, 2016.
- [7] Kacper Chwialkowski, Heiko Strathmann, and Arthur Gretton. A kernel test of goodness of fit. In *International Conference on Machine Learning*, 2016.
- [8] Jackson Gorham and Lester Mackey. Measuring sample quality with kernels. In *International Conference on Machine Learning*, 2017.
- [9] Andreas Anastasiou, Alessandro Barp, François-Xavier Briol, Bruno Ebner, Robert Gaunt, Fatemeh Ghaderinezhad, Jackson Gorham, Arthur Gretton, Christophe Ley, Qiang Liu, Lester Mackey, Chris Oates, Gesine Reinert, and Yvik Swan. Stein’s method meets statistics: a review of some recent developments. *arXiv:2105.03481*, 2021.
- [10] Li Wenliang and Heishiro Kanagawa. Blindness of score-based methods to isolated components and mixing proportions. *arXiv:2008.10087*, 2020.
- [11] Wenbo Gong, Yingzhen Li, and José Miguel Hernández-Lobato. Sliced kernelized Stein discrepancy. In *International Conference on Learning Representations*, 2021.
- [12] Jonathan Huggins and Lester Mackey. Random feature Stein discrepancies. In *Advances in Neural Information Processing Systems*, 2018.
- [13] Andrew Gelman and Donald Rubin. Inference from iterative simulation using multiple sequences. *Statistical Science*, 7(4):457–472, 1992.
- [14] Stephen Brooks and Andrew Gelman. General methods for monitoring convergence of iterative simulations. *Journal of Computational and Graphical Statistics*, 7(4):434–455, 1998.
- [15] John Geweke. Evaluating the accuracy of sampling-based approaches to the calculation of posterior moments. In J. M. Bernardo, J. O. Berger, and A. P. Dawid, editors, *Bayesian Statistics*, volume 4, pages 169–193, 1992.
- [16] Mary Kathryn Cowles and Bradley Carlin. Markov chain Monte Carlo convergence diagnostics: a comparative review. *Journal of the American Statistical Association*, 91(434):883–904, 1996.
- [17] Michael Jordan, Zoubin Ghahramani, Tommi Jaakkola, and Lawrence Saul. An introduction to variational methods for graphical models. *Machine Learning*, 37:183–233, 1999.
- [18] Martin Wainwright and Michael Jordan. Graphical models, exponential families, and variational inference. *Foundations and Trends in Machine Learning*, 1(1–2):1–305, 2008.
- [19] David Blei, Alp Kucukelbir, and Jon McAuliffe. Variational inference: a review for statisticians. *Journal of the American Statistical Association*, 112(518):859–877, 2017.
- [20] Danilo Rezende and Shakir Mohamed. Variational inference with normalizing flows. In *International Conference on Machine Learning*, 2015.

- [21] Rajesh Ranganath, Dustin Tran, and David Blei. Hierarchical variational models. In *International Conference on Machine Learning*, 2016.
- [22] George Papamakarios, Eric Nalisnick, Danilo Jimenez Rezende, Shakir Mohamed, and Balaji Lakshminarayanan. Normalizing flows for probabilistic modeling and inference. *Journal of Machine Learning Research*, 22:1–64, 2021.
- [23] Solomon Kullback and Richard Leibler. On information and sufficiency. *The Annals of Mathematical Statistics*, 22(1):79–86, 1951.
- [24] Matthew D. Hoffman, David M. Blei, Chong Wang, and John Paisley. Stochastic variational inference. *Journal of Machine Learning Research*, 14:1303–1347, 2013.
- [25] Rajesh Ranganath, Sean Gerrish, and David Blei. Black box variational inference. In *International Conference on Artificial Intelligence and Statistics*, 2014.
- [26] Tommi Jaakkola and Michael Jordan. Improving the mean field approximation via the use of mixture distributions. In *Learning in graphical models*, pages 163–173. Springer, 1998.
- [27] Samuel Gershman, Matthew Hoffman, and David Blei. Nonparametric variational inference. In *International Conference on Machine Learning*, 2012.
- [28] O. Zobay. Variational Bayesian inference with Gaussian-mixture approximations. *Electronic Journal of Statistics*, 8:355–389, 2014.
- [29] Fangjian Guo, Xiangyu Wang, Kai Fan, Tamara Broderick, and David Dunson. Boosting variational inference. In *Advances in Neural Information Processing Systems*, 2016.
- [30] Xiangyu Wang. Boosting variational inference: theory and examples. Master’s thesis, Duke University, 2016.
- [31] Andrew Miller, Nicholas Foti, and Ryan Adams. Variational boosting: iteratively refining posterior approximations. In *International Conference on Machine Learning*, 2017.
- [32] Francesco Locatello, Rajiv Khanna, Joydeep Ghosh, and Gunnar Rätsch. Boosting variational inference: an optimization perspective. In *International Conference on Artificial Intelligence and Statistics*, 2018.
- [33] Francesco Locatello, Gideon Dresdner, Rajiv Khanna, Isabel Valera, and Gunnar Rätsch. Boosting black box variational inference. In *Advances in Neural Information Processing Systems*, 2018.
- [34] Trevor Campbell and Xinglong Li. Universal boosting variational inference. In *Advances in Neural Information Processing Systems*, 2019.
- [35] Adrian Corduneanu and Christopher Bishop. Variational Bayesian model selection for mixture distributions. In *Artificial Intelligence and Statistics*, 2001.
- [36] Sato Masa-aki. Online model selection based on the variational Bayes. *Neural Computation*, 13(7):1649–1681, 2001.
- [37] Constantinos Constantinopoulos, Michalis Titsias, and Aristidis Likas. Bayesian feature and model selection for Gaussian mixture models. *IEEE Transactions on Pattern Analysis and Machine Intelligence*, 28(6):1013–1018, 2006.
- [38] John Ormerod, Chong You, and Samuel Müller. A variational Bayes approach to variable selection. *Electronic Journal of Statistics*, 11(2):3549–3594, 2017.
- [39] Badr-Eddine Chérif-Abdellatif and Pierre Alquier. Consistency of variational Bayes inference for estimation and model selection in mixtures. *Electronic Journal of Statistics*, 12(2):2995–3035, 2018.
- [40] Chenyang Tao, Liqun Chen, Ruiyi Zhang, Ricardo Henao, and Lawrence Carin. Variational inference and model selection with generalized evidence bounds. In *International Conference on Machine Learning*, 2018.
- [41] Zuheng Xu and Trevor Campbell. The computational asymptotics of variational inference and the Laplace approximation. *arXiv:2104.05886*, 2021.
- [42] Tim Salimans, Diederik Kingma, and Max Welling. Markov chain Monte Carlo and variational inference: bridging the gap. In *International Conference on Machine Learning*, 2015.

- [43] Christopher Wolf, Maximilian Karl, and Patrick van der Smagt. Variational inference with Hamiltonian Monte Carlo. *arXiv:1609.08203*, 2016.
- [44] Tomas Geffner and Justin Domke. MCMC variational inference via uncorrected Hamiltonian annealing. In *Advances in Neural Information Processing Systems*, 2021.
- [45] Guodong Zhang, Kyle Hsu, Jianing Li, Chelsea Finn, and Roger Grosse. Differentiable annealed importance sampling and the perils of gradient noise. In *Advances in Neural Information Processing Systems*, 2021.
- [46] Achille Thin, Nikita Kotelevskii, Alain Durmus, Maxim Panov, Eric Moulines, and Arnaud Doucet. Monte Carlo variational auto-encoders. In *International Conference on Machine Learning*, 2021.
- [47] Martin Jankowiak and Du Phan. Surrogate likelihoods for variational annealed importance sampling. *arXiv:2112.12194*, 2021.
- [48] Radford Neal. Hamiltonian importance sampling. Banff International Research Station (BIRS) Workshop on Mathematical Issues in Molecular Dynamics, 2005.
- [49] Anthony Caterini, Arnaud Doucet, and Dino Sejdinovic. Hamiltonian variational auto-encoder. In *Advances in Neural Information Processing Systems*, 2018.
- [50] Naitong Chen, Zuheng Xu, and Trevor Campbell. Bayesian inference via sparse Hamiltonian flows. *arXiv:2203.05723*, 2022.
- [51] Yichuan Zhang and José Miguel Hernández-Lobato. Ergodic inference: accelerate convergence by optimisation. In *International Conference on Learning Representations*, 2020.
- [52] Matthew Hoffman and Andrew Gelman. The No-U-Turn Sampler: adaptively setting path lengths in Hamiltonian Monte Carlo. *Journal of Machine Learning Research*, 15(1):1593–1623, 2014.
- [53] Esteban Tabak and Cristina Turner. A family of non-parametric density estimation algorithms. *Communications on Pure and Applied Mathematics*, 66(2):145–164, 2013.
- [54] Ivan Kobyzev, Simon Prince, and Marcus Brubaker. Normalizing flows: an introduction and review of current methods. *IEEE Transactions on Pattern Analysis and Machine Intelligence*, 43(11):3964–3979, 2021.
- [55] Tim Salimans and David Knowles. Fixed-form variational posterior approximation through stochastic linear regression. *Bayesian Analysis*, 8(4):837–882, 2013.
- [56] Diederik Kingma and Max Welling. Auto-encoding variational Bayes. In *International Conference on Learning Representations*, 2014.
- [57] Aılım Güneş Baydin, Barak Pearlmutter, Alexey Radul, and Jeffrey Siskind. Automatic differentiation in machine learning: a survey. *Journal of Machine Learning Research*, 18:1–43, 2018.
- [58] Tanja Eisner, Bálint Farkas, Markus Haase, and Rainer Nagel. *Operator Theoretic Aspects of Ergodic Theory*. Graduate Texts in Mathematics. Springer, 2015.
- [59] Karma Dajani and Sjoerd Dirksin. A simple introduction to ergodic theory, 2008. URL: <https://webspace.science.uu.nl/kraai101/lecturenotes2009.pdf>.
- [60] George Birkhoff. Proof of the ergodic theorem. *Proceedings of the National Academy of Sciences*, 17(12): 656–660, 1931.
- [61] Gareth Roberts and Jeffrey Rosenthal. Shift-coupling and convergence rates of ergodic averages. *Stochastic Models*, 13(1):147–165, 1997.
- [62] David Aldous and Hermann Thorisson. Shift-coupling. *Stochastic Processes and their Applications*, 44: 1–14, 1993.
- [63] Grant Rotskoff and Eric Vanden-Eijnden. Dynamical computation of the density of states and Bayes factors using nonequilibrium importance sampling. *Physical Review Letters*, 122(15):150602, 2019.
- [64] Achille Thin, Yazid Janati, Sylvain Le Corff, Charles Ollion, Arnaud Doucet, Alain Durmus, Éric Moulines, and Christian Robert. NEO: non equilibrium sampling on the orbit of a deterministic transform. *arXiv:2103.10943*, 2021.
- [65] Sergio Verdú. Total variation distance and the distribution of the relative information. In *IEEE Information Theory and Applications Workshop*, 2014.

- [66] Radford Neal. MCMC using Hamiltonian dynamics. In Steve Brooks, Andrew Gelman, Galin Jones, and Xiao-Li Meng, editors, *Handbook of Markov chain Monte Carlo*, chapter 5. CRC Press, 2011.
- [67] Radford Neal. How to view an MCMC simulation as permutation, with applications to parallel simulation and improved importance sampling. *arXiv:1205.0070*, 2012.
- [68] Iain Murray and Lloyd Elliott. Driving Markov chain Monte Carlo with a dependent random stream. *arXiv:1204.3187*, 2012.
- [69] Radford Neal. *Bayesian Learning for Neural Networks*. Lecture Notes in Statistics, No. 118. Springer-Verlag, 1996.
- [70] Heikki Haario, Eero Saksman, and Johanna Tamminen. An adaptive Metropolis algorithm. *Bernoulli*, pages 223–242, 2001.
- [71] Radford Neal. Slice sampling. *The Annals of Statistics*, 31(3):705–767, 2003.
- [72] David Harrison Jr. and Daniel Rubinfeld. Hedonic housing prices and the demand for clean air. *Journal of Environmental Economics and Management*, 5(1):81–102, 1978.
- [73] Sérgio Moro, Paulo Cortez, and Paulo Rita. A data-driven approach to predict the success of bank telemarketing. *Decision Support Systems*, 62:22–31, 2014.
- [74] Kirill Neklyudov, Max Welling, Evgenii Egorov, and Dmitry Vetrov. Involutive MCMC: a unifying framework. In *International Conference on Machine Learning*, 2020.
- [75] Span Spanbauer, Cameron Freer, and Vikash Mansinghka. Deep involutive generative models for neural MCMC. *arXiv:2006.15167*, 2020.
- [76] Kirill Neklyudov and Max Welling. Orbital MCMC. In *Artificial Intelligence and Statistics*, 2022.
- [77] Kôzaku Yosida. Mean ergodic theorem in Banach spaces. *Proceedings of the Imperial Academy*, 14(8): 292–294, 1938.
- [78] Shizuo Kakutani. Iteration of linear operations in complex Banach spaces. *Proceedings of the Imperial Academy*, 14(8):295–300, 1938.
- [79] Frigyes Riesz. Some mean ergodic theorems. *Journal of the London Mathematical Society*, 13(4):274–278, 1938.

A Proofs

Proof of Theorem 3.1. Since setwise convergence implies weak convergence, we will focus on proving setwise convergence. We have that $q_{\lambda, N}$ converges setwise to π if and only if for all measurable bounded $f : \mathcal{X} \rightarrow \mathbb{R}$,

$$\mathbb{E}f(X_N) \rightarrow \mathbb{E}f(X), \quad X_N \sim q_{\lambda, N}, \quad X \sim \pi.$$

The proof proceeds by directly analyzing $\mathbb{E}f(X_N)$:

$$\begin{aligned} \mathbb{E}f(X_N) &= \int f(x)q_{\lambda, N}(dx) \\ &= \frac{1}{N} \sum_{n=0}^{N-1} \int f(x)(T_{\lambda}^n q_0)(dx) \\ &= \frac{1}{N} \sum_{n=0}^{N-1} \int f(T_{\lambda}^n x)q_0(dx) \\ &= \int \frac{1}{N} \sum_{n=0}^{N-1} f(T_{\lambda}^n x)q_0(dx). \end{aligned}$$

Since $q_0 \ll \pi$, by the Radon-Nikodym theorem, there exists a density of q_0 with respect to π , so

$$\mathbb{E}f(X_N) = \int \frac{1}{N} \sum_{n=0}^{N-1} f(T_{\lambda}^n x) \frac{dq_0}{d\pi}(x) \pi(dx).$$

By the pointwise ergodic theorem (Theorem 2.3), $f_N(x) = \frac{1}{N} \sum_{n=0}^{N-1} f(T_\lambda^n x)$ converges pointwise π -a.e. to $\int f d\pi$; and because f is bounded, f_N is uniformly bounded for all $N \in \mathbb{N}$. Hence by the Lebesgue dominated convergence theorem,

$$\begin{aligned} \lim_{N \rightarrow \infty} \mathbb{E}f(X_N) &= \lim_{N \rightarrow \infty} \int \frac{1}{N} \sum_{n=0}^{N-1} f(T_\lambda^n x) \frac{dq_0}{d\pi}(x) \pi(dx) \\ &= \int \left(\int f d\pi \right) \frac{dq_0}{d\pi}(x) \pi(dx) \\ &= \left(\int f d\pi \right) \cdot 1 = \mathbb{E}f(X). \end{aligned}$$

□

Theorem A.1 (Mean ergodic theorem in Banach spaces [77–79; 58, Theorem 8.5]). *Let T be a bounded linear operator on a Banach space E , define the operator*

$$A_N = \frac{1}{N} \sum_{n=0}^{N-1} T^n,$$

and let

$$\text{fix}(T) = \{v \in E : Tv = v\} = \ker(I - T).$$

Suppose that $\sup_{N \in \mathbb{N}} \|A_N\| < \infty$ and that $\frac{1}{N} T^N v \rightarrow 0$ for all $v \in E$. Then the subspace

$$V = \left\{ v \in E : \lim_{N \rightarrow \infty} A_N v \text{ exists} \right\}$$

is closed, T -invariant, and decomposes into a direct sum of closed subspaces

$$V = \text{fix}(T) \oplus \overline{\text{range}}(I - T).$$

The operator $T|_V$ on V is mean ergodic. Furthermore, the operator

$$A : V \rightarrow \text{fix}(T) \quad Av = \lim_{N \rightarrow \infty} A_N v$$

is a bounded projection with kernel $\ker(A) = \overline{\text{range}}(I - T)$ and $AT = A = TA$.

Proof of Theorem 3.2. Denote μ to be the Lebesgue measure on \mathbb{R}^d , and consider the Banach space $L^1(\mu)$ and linear operator T on $L^1(\mu)$ defined by

$$Tf = \frac{f(T^{-1}(x))}{J(T^{-1}(x))},$$

where $J(x)$ is the Jacobian determinant of $T(x)$. We suppress λ subscripts for brevity, and note the slight abuse of notation involving the same symbol for $T : \mathcal{X} \rightarrow \mathcal{X}$ the associated operator. By a simple change of variables,

$$\|Tf\|_1 = \int |Tf(x)| \mu(dx) = \int |f(x)| \mu(dx) = \|f\|_1,$$

and so T is bounded with $\|T\| = 1$. Hence $\frac{1}{N} T^N f \rightarrow 0$ for all $f \in L^1(\mu)$, and if we define the operator

$$\forall N \in \mathbb{N}, \quad A_N = \frac{1}{N} \sum_{n=0}^{N-1} T^n,$$

we have that $\sup_{N \in \mathbb{N}} \|A_N\| \leq 1$. Therefore by the mean ergodic theorem in Banach spaces [77–79; 58, Theorem 8.5], we have that

$$A : E \rightarrow \text{fix}(T) \quad Af = \lim_{N \rightarrow \infty} A_N f$$

where $E = \{f \in L^1(\mu) : \lim_{N \rightarrow \infty} A_N f \text{ exists}\}$. [58, Theorem 8.20] guarantees that $E = L^1(\mu)$ as long as the weak limit of $A_N f$ exists for each $f \in L^1(\mu)$. Note that since μ is σ -finite, the dual space of $L^1(\mu)$ is the set of linear functionals

$$f \mapsto \int f(x) \phi(x) \mu(dx), \quad \phi \in L^\infty(\mu).$$

So therefore we have that $E = L^1(\mu)$ if for each $f \in L^1(\mu)$, there exists a $g \in L^1(\mu)$ such that

$$\forall \phi \in L^\infty(\mu), \quad \int (A_N f)(x) \phi(x) \mu(dx) \rightarrow \int g(x) \phi(x) \mu(dx).$$

The same technique using a transformation of variables and the pointwise ergodic theorem from the proof of Theorem 3.1 provides the desired weak convergence. Therefore we have L^1 convergence to $\text{fix}(T)$ and hence total variation convergence to an element of $\text{fix}(T)$. Since $q_0 \ll \pi$, Theorem 3.1 guarantees weak convergence to π ; and since we know $A_N f \rightarrow \text{fix}(T)$ and $\pi \in \text{fix}(T)$, we have that $D_{\text{TV}}(q_{\lambda, N}, \pi) \rightarrow 0$. □

Proposition A.2 ([65, Theorem 7]). *Suppose q, π are two probability distributions on \mathcal{X} such that $q \ll \pi$ and both have a density with respect to a common base measure. If*

$$\alpha = \sup_{x \in \mathcal{X}} \frac{q(x)}{\pi(x)} < \infty,$$

then

$$D_{\text{TV}}(q, \pi) \geq \frac{\alpha - 1}{2\alpha \log \alpha} D_{\text{KL}}(q || \pi).$$

Proof. We provide a proof for completeness. The KL divergence is

$$D_{\text{KL}}(q || \pi) = \int q(x) \log \frac{q(x)}{\pi(x)} dx = \int \pi(x) \frac{q(x)}{\pi(x)} \log \frac{q(x)}{\pi(x)} dx.$$

Note that $\alpha \geq 1$ by definition, and that

$$\forall y \in [0, \alpha], \quad \frac{\alpha \log \alpha}{\alpha - 1} |y - 1| \geq y \log y.$$

Therefore

$$D_{\text{KL}}(q || \pi) \leq \frac{\alpha \log \alpha}{\alpha - 1} \int \pi(x) \left| \frac{q(x)}{\pi(x)} - 1 \right| dx = \frac{2\alpha \log \alpha}{\alpha - 1} \frac{1}{2} \int |q(x) - \pi(x)| dx = \frac{2\alpha \log \alpha}{\alpha - 1} D_{\text{TV}}(q, \pi).$$

□

B Hamiltonian flow pseudocode

Algorithm 4 Compute T_λ and J_λ for Hamiltonian flow

Require: initial state $x \in \mathcal{X}$, $\rho \in \mathbb{R}^d$, $u \in [0, 1]$, step size ϵ , shift $\xi \in \mathbb{R}$, pseudorandom shift $z(\cdot, \cdot)$

```

 $x_0, \rho_0 \leftarrow x, \rho$ 
for  $\ell = 1, \dots, L$  do
     $x_\ell, \rho_\ell \leftarrow \hat{H}_\epsilon(x_{\ell-1}, \rho_{\ell-1})$ 
end for
 $x', \rho' \leftarrow x_L, \rho_L$ 
 $u' \leftarrow u + \xi \pmod{1}$ 
for  $i = 1, \dots, d$  do
     $\rho''_i \leftarrow R^{-1}(R(\rho'_i) + z(x'_i, u')) \pmod{1}$ 
end for
 $J \leftarrow m(\rho') / m(\rho'')$ 
return  $(x', \rho'', u'), J$ 

```

C Extensions

Tunable reference So far we have assumed that the reference distribution q_0 for the flow is fixed. Given that q_0 is often quite far from the target π , this forces the variational flow to spend some of its steps just moving the bulk of the mass to π . But this can be accomplished much easier with, say, a simple linear transformation that efficiently allows large global moves in mass. For example, if $q_0 = \mathcal{N}(0, I)$, we can include a map M_θ

$$q_{\lambda, N} = \frac{1}{N} \sum_{n=0}^{N-1} T_\lambda^n M_\theta q_0,$$

where $M_\theta(x) = \theta_1 x + \theta_2$, where $\theta_1 \in \mathbb{R}^{d \times d}$ and $\theta_2 \in \mathbb{R}^d$. Note that it is possible to optimize the reference and flow jointly, or to optimize the reference distribution by itself first and then use that fixed reference in the flow optimization.

Automated burn-in A common practice in MCMC is to throw away a first fraction of the states in the sequence to ensure that the starting sample is in a high probability region of the target distribution, thus reducing the bias from initialization (“burn-in”). Usually one needs a diagnostic to check when burn-in is completed. In

the case of ErgFlow, we can monitor the burn-in phase in a principled way by evaluating the ELBO. Once the flow is trained, the variational distribution with M burn-in samples is simply

$$q_{\lambda, M, N} = \frac{1}{N - M} \sum_{n=M}^{N-1} T_{\lambda}^n q_0,$$

We can easily optimize this by estimating the ELBOs for $M = 1, \dots, N$.

Mixed flows One can build multiple flows starting from multiple different initial reference distributions; when the posterior is multimodal, it may be the case that some of these flows converge to different modes but do not mix across modes. In this scenario, it can be helpful to mix several flows, i.e., build an approximation of the form

$$q_{\lambda, N}^* = \sum_{k=1}^K w_k (q_{\lambda, N})_k, \quad \sum_{k=1}^K w_k = 1.$$

Because each component flow provides access to i.i.d. samples and density evaluation, ErgFlow provides the ability to optimize the weights by maximizing the ELBO (i.e., minimizing the KL divergence).

D Additional experimental details

In this section, we provide details for each experiment presented in the main text, as well as additional results regarding numerical stability and a high-dimensional synthetic experiment. Aside from the univariate synthetic example, all examples include a pseudotime shift step with $\xi = \pi/16$, and a momentum refreshment with $z(x, u) = 0.5 \sin(2x + u) + 0.5$. For the kernel Stein discrepancy, we use a Gaussian kernel $k(x, y) = \exp(-\frac{1}{h} \|x - y\|^2)$ with bandwidth h set to the median of the pairwise squared Euclidean distances between samples, as suggested in [6]. For all experiments, unless otherwise stated, NUTS uses 10,000 steps for adaptation, targeting at an average acceptance ratio 0.7, and generates 5,000 samples for KSD estimation. The KSD for ErgFlow is estimated using 2,000 samples.

D.1 Univariate synthetic examples

The three target distributions tested in this experiment were

- normal: $\mathcal{N}(2, 2^2)$,
- synthetic Gaussian mixture: $0.5\mathcal{N}(-3, 1.5^2) + 0.3\mathcal{N}(0, 0.8^2) + 0.2\mathcal{N}(3, 0.8^2)$, and
- Cauchy: $\text{Cauchy}(0, 1)$.

For all three examples, we use a momentum refreshment without introducing the pseudotime variable; this enables us to plot the full joint density of $(x, \rho) \in \mathbb{R}^2$:

$$\rho'' \leftarrow R_{\text{Lap}}^{-1}(R_{\text{Lap}}(\rho') + (\sin(2x') + 1)/2 \pmod{1}).$$

For the three examples, we used the leapfrog stepsize $\epsilon = 0.05$ and run $L = 50$ leapfrogs between each refreshment. For both the Gaussian and Gaussian mixture targets, we use 100 refreshments. In the case of the Cauchy, we used 1,000 refreshments.

D.2 Multivariate synthetic examples

The three target distributions tested in this experiment were

- the banana distribution [70]:

$$y = \begin{bmatrix} y_1 \\ y_2 \end{bmatrix} \sim \mathcal{N}\left(0, \begin{bmatrix} 100 & 0 \\ 0 & 1 \end{bmatrix}\right), \quad x = \begin{bmatrix} y_1 \\ y_2 - by_1 + 100b \end{bmatrix}, \quad b = 0.1;$$

- Neals' funnel [71]:

$$x_1 \sim \mathcal{N}\left(\frac{\sigma^2}{4}, \sigma^2\right), \quad x_2 | x_1 \sim \mathcal{N}\left(0, \exp\left(\frac{x_1}{2}\right)\right), \quad \sigma^2 = 36;$$

- a cross-shaped distribution: in particular, a Gaussian mixture of the form

$$\begin{aligned} x \sim & \frac{1}{4} \mathcal{N}\left(\begin{bmatrix} 0 \\ 2 \end{bmatrix}, \begin{bmatrix} 0.15^2 & 0 \\ 0 & 1 \end{bmatrix}\right) + \frac{1}{4} \mathcal{N}\left(\begin{bmatrix} -2 \\ 0 \end{bmatrix}, \begin{bmatrix} 0 & 0 \\ 0.15^2 & 0 \end{bmatrix}\right) \\ & + \frac{1}{4} \mathcal{N}\left(\begin{bmatrix} 2 \\ 0 \end{bmatrix}, \begin{bmatrix} 0 & 0 \\ 0.15^2 & 1 \end{bmatrix}\right) + \frac{1}{4} \mathcal{N}\left(\begin{bmatrix} 0 \\ -2 \end{bmatrix}, \begin{bmatrix} 0.15^2 & 0 \\ 0 & 1 \end{bmatrix}\right); \end{aligned}$$

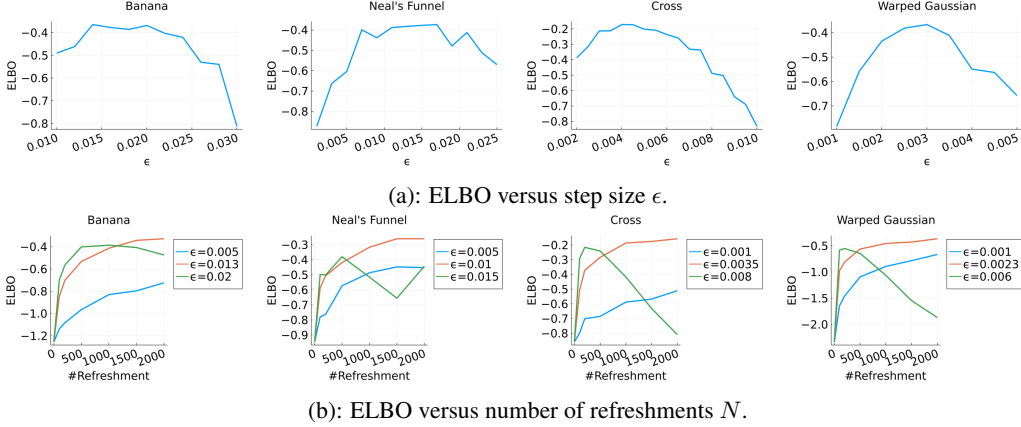


Figure 5: Tuning for the four multivariate synthetic examples.

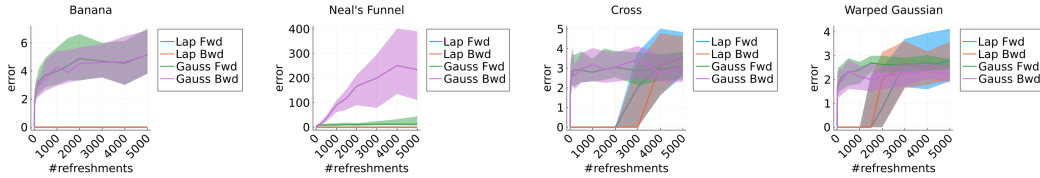


Figure 6: Stability of composing $T_\lambda^{-K} \circ T_\lambda^K$ (Fwd) and $T_\lambda^K \circ T_\lambda^{-K}$ (Bwd) for the four multivariate experiments with flows constructed using Gaussian (Gauss) and Laplace (Lap) momentum distributions. The vertical axis shows the 2-norm error of reconstructing (x, ρ, u) sampled from q_0 ; the horizontal axis shows increasing numbers of refreshments K . The lines indicate the median, and error regions indicate 25th to 75th percentile for 100 independent samples.

- and a warped Gaussian distribution

$$y = \begin{bmatrix} y_1 \\ y_2 \end{bmatrix} \sim \mathcal{N}\left(0, \begin{bmatrix} 1 & 0 \\ 0 & 0.12^2 \end{bmatrix}\right), \quad x = \begin{bmatrix} \|y\|_2 \cos\left(\text{atan2}(y_2, y_1) + \frac{1}{2}\|y\|_2\right) \\ \|y\|_2 \sin\left(\text{atan2}(y_2, y_1) + \frac{1}{2}\|y\|_2\right) \end{bmatrix},$$

where $\text{atan2}(y, x)$ is the angle, in radians, between the positive x axis and the ray to the point (x, y) .

For each target distribution we used a flow with 1,000 refreshments; between each refreshment we used 50 leapfrog steps for the banana distribution, 60 for the cross distribution, and 80 for the funnel and warped Gaussian. Note that in all four examples, we individually tuned the step size ϵ by maximizing the estimated ELBO, as shown in Fig. 5a. Fig. 5b also demonstrates how the ELBO varies versus the number of refreshments N . For small step sizes ϵ , the discretized Hamiltonian dynamics approximates the continuous dynamics, and the ELBO generally increases with N indicating convergence to the target. For larger step sizes ϵ , the ELBO increases to a peak and then decreases, indicating that the discretized dynamics do not exactly target the desired distribution.

Fig. 6 shows why we opted to use a Laplace momentum distribution as opposed to a Gaussian momentum. In particular, the numerical error of composing $T_\lambda^K \circ T_\lambda^{-K}$ and $T_\lambda^{-K} \circ T_\lambda^K$ (denoted as ‘‘Bwd’’ and ‘‘Fwd’’ in the legend, respectively) indicate that the flow using the Laplace momentum is more reliably invertible for larger numbers of refreshments than the flow with a Gaussian momentum. This is largely due to the fact that the normal has very light tails; for example, for large momentum values in the right tail, the CDF is ≈ 1 , which gets rounded to exactly 1 in floating point representation. Note that our implementation of the CDF and inverse CDF was fairly naïve; more stable computation could be achieved with more care taken to prevent rounding.

Finally, Fig. 7 provides a more comprehensive set of sample histograms for these experiments, showing the x -, ρ -, and u -marginals. It is clear that ErgFlow generates samples for each variable reliably from the target marginal.

D.3 Bayesian linear and logistic regression

For linear regression, we standardize all features and the response of the dataset. For logistic regression, we include 8 features from the bank marketing dataset [73]: client age, marital status, balance, housing loan status, duration of last contact, number of contacts during campaign, number of days since last contact, and number of

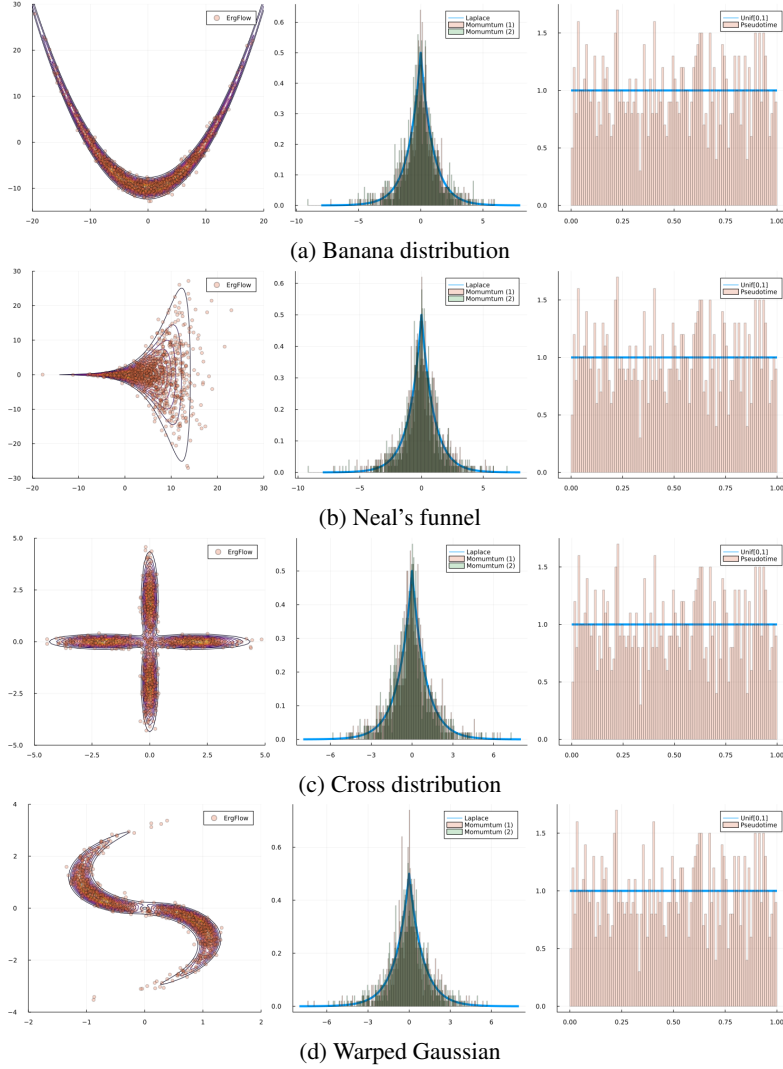


Figure 7: Scatter plots and histograms for the x -, ρ -, and u -marginals in the four synthetic experiments.

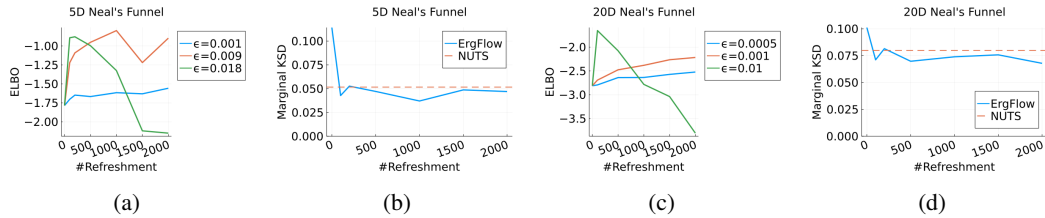


Figure 8: ELBO versus step size (8a,8c) and KSD comparison with NUTS (8b,8d) for the 5- and 20-dimensional Neal's funnel examples.

contacts before the current campaign. For each of the binary variables (marital status and housing loan status), all unknown entries are removed. All features of the dataset are also standardized.

For both examples, we initialize ErgFlow at $q_0 = \mathcal{N}(0, 0.01I)$. NUTS uses 20,000 steps for adaptation, with a targeted average acceptance ratio 0.7. The KSDs for both ErgFlow and NUTS are estimated using 5,000 samples, and ELBOs are based on 5,000 samples as well. Between refreshments, we use 30 leapfrog steps for the linear regression example, and 50 for the logistic regression example. The leapfrog stepsize ϵ of ErgFlow used in KSD comparison against NUTS (Figs. 4b and 4d) are selected to be the optimal ones from the ELBO comparison plots (Figs. 4a and 4c) respectively.

D.4 Higher-dimensional synthetic experiment

We also tested two higher dimensional Neal’s funnel target distributions of $x \in \mathbb{R}^d$ where $d = 5, 20$. In particular, we used the target distribution

$$x_1 \sim \mathcal{N}\left(\frac{\sigma^2}{4}, \sigma^2\right), \quad \text{and} \quad \forall i \in \{2, \dots, d\}, x_i | x_1 \stackrel{\text{i.i.d.}}{\sim} \mathcal{N}\left(0, \exp\left(\frac{x_1}{2}\right)\right),$$

with $\sigma^2 = 36$. We use 80 leapfrogs between refreshments and $\epsilon = 0.0009$ when $d = 5$, and 100 leapfrogs between refreshments and $\epsilon = 0.001$ when $d = 20$ (Figs. 8a and 8c shows the ELBO comparison used to tune the step size ϵ). Figs. 8b and 8d confirm via the KSD that the method performs as well as NUTS in higher-dimensional cases.